Noname manuscript No.
(will be inserted by the editor)

High-performance Parallel Solver for Integral Equations of Electromagnetics Based on Galerkin Method

Mikhail Kruglyakov · Lidia Bloshanskaya

Received: / Accepted:

Abstract A new parallel solver for the volumetric integral equations (IE) of electrodynamics is presented. The solver is based on the Galerkin method which ensures the convergent numerical solution. The main features include: (i) the reduction of the memory usage in 8 times, compared to analogous IE based algorithms, without additional restriction on the background media; (ii) accurate and stable method to compute matrix coefficients corresponding to the IE; (iii) high degree of parallelism. The solver's computational efficiency is shown on a problem of magnetotelluric sounding

Mikhail Kruglyakov (✉)

Faculty of Computational Mathematics and Cybernetics, Lomonosov MSU, GSP-1,

Leninskiye Gory, 1-52, 119991 Moscow, Russia

Tel. +74959391919 Fax. +74959392596

Institute of Geophysics, ETH Zurich, Sonneggstrasse 5, 8092 Zurich, Switzerland

E-mail: mkruglyakov@cs.msu.su

Lidia Bloshanskaya

SUNY New Paltz, Department of Mathematics, 1 Hawk Dr, New Paltz, NY 12561, U.S.A.

E-mail: bloshanl@newpaltz.edu

of the high conductivity contrast media. A good agreement with the results obtained with the second order finite element method is demonstrated. Due to effective approach to parallelization and distributed data storage the program exhibits perfect scalability on different hardware platforms.

Keywords Integral equations · Forward modeling · Electromagnetic sounding · Galerkin method · Green's tensor · High-performance computing

1 Introduction

Electromagnetic (EM) methods of geophysics are used to model the subsurface electrical conductivity distribution. Conductivity is affected by the rock type and composition, temperature, and fluid/melt content and thus can be used in various engineering and industrial problems like detecting hydrocarbon (low-conductive) and geothermal or ore (high-conductive) reservoirs. Measured electrical and/or magnetic fields are further interpreted via the calculations for a given three-dimensional model of conductivity distribution. Maxwell's equation describing the EM field distribution can not be solved analytically in general case requiring numerical simulation. Large number of such simulations is required, and complex large scale models are invoked, Chave and Jones (2012).

The growing amount of data calls for the development of new numerical methods capable to deliver fast and accurate EM simulations and harness computational power provided by modern high-performance multi-core and multi-node platforms.

Nowadays most of the numerical solvers for Maxwell's equations are based on the finite element (FE), Börner (2010), or the integral equations (IE), Pankratov and

Kuvshinov (2016), methods. The main difference between these methods is that in FE discretization results in large sparse systems, Ernst and Gander (2012), while in the IE methods one works with compact dense system matrices. The compactness in IE is achieved since the boundary conditions are exactly accounted for via Green's functions, and thus the modeling region is confined only to the three-dimensional conductivity structures (anomalies) under investigations, Raiche (1974); Weidelt (1975). Note that usually model consists of a number of nonuniform three-dimensional anomalies embedded in the one-dimensional (layered) background media. By contrast, in the FE methods one has to discretize a much larger volume both in lateral and vertical directions in order to enable the decay (or stabilization) of the EM field at the boundaries of the modeling domain, Grayver and Kolev (2015); Mulder (2006). Another distinction between these methods is that the condition number of matrices (which controls the stability of the solution) in FE depends on discretization and frequency, whereas in IE approach practically does not, Pankratov et al (1995); Singer (1995).

The main focus in development and implementation of the numerical methods for the IE is the efficiency and performance for the large number of unknown parameters. The proposed new iterative numerical solver for the IE addresses this issue both mathematically (increasing the accuracy and stability of coefficient computations and reducing the memory usage) and computationally (allowing high degree of parallelism without memory loss at the nodes). The special class of integral equations is used: the integral equations with contracting kernel (CIE), Pankratov et al (1995); Singer (1995). It was proved that CIE have unique solution and their system matrix is well-conditioned by construction, Pankratov et al (1995); Singer (1995). The

Galerkin method is used to solve CIE numerically, Delves and Mohamed (1985). In Kruglyakov (2011); Singer (2008) it was proved that the corresponding solution converges.

Two main cornerstones in the IE numerical solution are the calculation of matrix coefficients with sufficient accuracy, Wannmaker (1991), and the storage of this dense matrix in some packed form, Avdeev et al (1997, 2002). The Galerkin method with piece-wise constant basis allows to address both of these topics. Namely, the system matrix is decomposed into sums and multiplications of diagonal and block-Toeplitz matrices. First, matrix coefficients (i.e., double volumetric integrals of the product of basis functions and CIE kernel) are analytically transformed into one-dimensional convolution integrals. Then these convolution integrals are computed by digital filtering approach. Note, that only weights of these filters are computed numerically, whereas the functions in the knots are computed analytically. The resulting system is solved using the Flexible GMRES, Saad (1993), in parallel implementation by Fraysse et al (2003).

The proposed solver possesses three main features: 1) Reduction of the memory usage in 8 times, compared to analogous IE solving algorithms. It is important to stress that the memory is saved for any background with an arbitrary number of layers. In contrast, in Kamm and Pedersen (2014) the memory reduction is achieved only in case of homogenous half-space as a background and uniform vertical discretization. In Avdeev and Knizhnik (2009); Koyama et al (2008); Sun and Kuvshinov (2015) it is achieved at the expense of accuracy and performance. The idea behind is to combine the Galerkin method with the properties of EM field, namely Lorentz

reciprocity. The matrix of the ensuing linear system can be broken in symmetric and antisymmetric submatricies resulting in the reduction of memory requirements in 8 times, Sect. 3. 2) Efficient and accurate method for the computation of these matrices, Sect. 3. 3) The implementation with high degree of parallelism. The computational experiments performed with "Bluegene" and "Lomonosov" supercomputers from MSU, and high-performance computer (HPC) "Piz Daint" from Swiss National Supercomputing Center show that the solver makes the best usage of 128 to 2,048 nodes for calculation at a single frequency and a single source. The program exhibits perfect scalability.

This paper is organized as follows. Section 2 is devoted to the overview of the CIE approach and the construction of the approximating system of linear equations. Section 3 addresses the reduction in memory requirements, the computation of matrix coefficients, and features of parallel implementation. In Sect. 4 the computational results for high (more than $3 \cdot 10^4$) conductivity contrast COMMEMI3D-3 model (Hursan and Zhdanov (2002); Varentsov et al (2000)) are compared with the corresponding results obtained using FE method by Grayver and Kolev (2015). The Appendices A to C provide the mathematical details of the presented method.

2 Contracting Integral Equation

2.1 Overview

Assume that the EM fields are induced by the external electric currents $\mathbf{J}_{ext}$. Moreover, assume that the EM fields are time dependent as $e^{-i\omega t}$, where ω is an angu-

lar frequency, $i = \sqrt{-1}$ and magnetic permeability μ_0 is the same in whole space. Let $\sigma(M)$, $\mathbf{Re}\,\sigma(M) \geq 0$ be a three-dimensional complex conductivity distribution in space. Then the electrical field $\mathbf{E}$ and the magnetic field $\mathbf{H}$ give the solution of the system of Maxwell's equations

$$\begin{cases} \operatorname{curl}\mathbf{H} = \sigma\mathbf{E} + \mathbf{J}_{ext}, \\ \operatorname{curl}\mathbf{E} = i\omega\mu_0\mathbf{H}. \end{cases} \tag{1}$$

The solution of (1) is unique under the additional radiation conditions at infinity, Ward and Hohmann (1988).

Let $\Omega \subset \mathbf{R}^3$ be some bounded domain and $\sigma(M) = \sigma_b(z)$ for $M(x,y,z) \notin \Omega$ and $\sigma(M) = \sigma_a(M)$ for $M \in \Omega$ (Fig. 1). Then for any $M \in \mathbf{R}^3$ the fields $\mathbf{E}(M)$ and $\mathbf{H}(M)$ are expressed in terms of the integrals

$$\begin{aligned} \mathbf{E}(M) &= \mathbf{E}^N(M) + \int\limits_{\Omega} \widehat{G}^E(M,M_0)\,(\sigma_a(M_0) - \sigma_b(M_0))\,\mathbf{E}(M_0)\,d\Omega_{M_0}, \\ \mathbf{H}(M) &= \mathbf{H}^N(M) + \int\limits_{\Omega} \widehat{G}^H(M,M_0)\,(\sigma_a(M_0) - \sigma_b(M_0))\,\mathbf{E}(M_0)\,d\Omega_{M_0}. \end{aligned} \tag{2}$$

Here $\widehat{G}^E$, $\widehat{G}^H$ are electrical and magnetic Green's tensors respectively, Dmitriev et al (2002); Pankratov et al (1995). The terms $\mathbf{E}^N$, $\mathbf{H}^N$ are called the normal electric and magnetic fields, corresponding. They form the solution of the system

$$\begin{cases} \operatorname{curl}\mathbf{H}^N = \sigma_b(z)\mathbf{E}^N + \mathbf{J}_{ext}, \\ \operatorname{curl}\mathbf{E}^N = i\omega\mu_0\mathbf{H}^N \end{cases} \tag{3}$$

with corresponding conditions at the infinity. Note, that $\widehat{G}^E$, $\widehat{G}^H$ are indepent of the anomalous conductivity σ_a.

Let $\mathbf{L}_2[\Omega]$ be a Hilbert functional space of vector functions $\mathbf{V}$ with the following norm and dot product

$$\begin{aligned}(\mathbf{V},\mathbf{U})_{\mathbf{L}_2[\Omega]} &= \int\limits_{\Omega} \left(V_x(M)\overline{U}_x(M)+V_y(M)\overline{U}_y(M)+V_z(M)\overline{U}_z(M)\right) d\Omega_M,\\ \|\mathbf{V}\|_{\mathbf{L}_2[\Omega]} &= \sqrt{(\mathbf{V},\mathbf{V})}.\end{aligned} \tag{4}$$

Suppose $\mathbf{Re}\,\sigma_b(z) > 0$ for $M(x,y,z) \in \Omega$ (the typical EM sounding situation), then the operator $\mathbf{G}_{\mathrm{E}}^{\mathrm{m}}$ is defined as

$$\mathbf{G}_{\mathrm{E}}^{\mathrm{m}}\mathbf{V} = \sqrt{\mathbf{Re}\,\sigma_b}\,\widehat{\mathrm{G}}^{\mathrm{E}}\left[2\sqrt{\mathbf{Re}\,\sigma_b}\mathbf{V}\right] + \mathbf{V}, \tag{5}$$

where $\widehat{\mathrm{G}}^{\mathrm{E}}$ is an integral operator from the first equation in (2). The operator $\mathbf{G}_{\mathrm{E}}^{\mathrm{m}}$ is a contracting operator in $\mathbf{L}_2[\Omega]$, Pankratov et al (1995); Singer (1995). Using (2) and (5) one obtains the CIE for $\mathbf{E}$

$$\begin{aligned}&\left(\mathrm{I}-\mathbf{G}_{\mathrm{E}}^{\mathrm{m}}\frac{b}{a}\right)\widetilde{\mathbf{E}} = \sqrt{\mathbf{Re}\,\sigma_b}\mathbf{E}^N,\\ &\widetilde{\mathbf{E}} = a\mathbf{E}, \quad a = \frac{\sigma_a+\overline{\sigma_b}}{2\sqrt{\mathbf{Re}\,\sigma_b}} \quad b = \frac{\sigma_a-\sigma_b}{2\sqrt{\mathbf{Re}\,\sigma_b}},\end{aligned} \tag{6}$$

where I is the identity operator and $\overline{\sigma_b}$ means complex conjugation of σ_b.

2.2 Galerkin Method

Suppose the domain Ω is divided in nonoverlapping subdomains $\Omega = \cup\Omega_n$, $n = 1\ldots N$ and $\sigma_b(M) = \sigma_b^n$, $\sigma_a(M) = \sigma_a^n$ for $M \in \Omega_n, n = 1\ldots N$. For each subdomain Ω_n define the function $W_n(M)$ as

$$W_n(M) = \begin{cases}\dfrac{1}{V_n},\ M \in \Omega_n,\\ 0,\ M \notin \Omega_n,\end{cases} \qquad V_n = \int\limits_{\Omega_n} d\Omega_M, \quad n = 1\ldots N. \tag{7}$$

Let $\widetilde{\mathbf{W}}^N$ be a linear span of the vector functions $\mathbf{W}_n$, $\mathbf{W}_n = (W_{n_x}, W_{n_y}, W_{n_z})$, $n_x, n_y, n_z = 1 \dots N$ and $\mathbf{P}^{\mathrm{N}}$ be a projection operator from $\mathbf{L}_2[\Omega]$ to $\widetilde{\mathbf{W}}^N$

$$\forall \mathbf{F} \in \mathbf{L}_2[\Omega] \quad \left[\mathbf{P}^{\mathrm{N}}[\mathbf{F}]\right]_\gamma = \sum_{n=1}^{N} \alpha_n^\gamma W_n, \quad \alpha_n^\gamma = \frac{\int\limits_{\Omega_n} F_\gamma(M) d\Omega_M}{V_n}, \tag{8}$$

where $\gamma = x, y, z$. Note that $\left\|\mathbf{P}^{\mathrm{N}}\right\| = 1$.

Applying $\mathbf{P}^{\mathrm{N}}$ to the first equation in (6) one obtains the operator equation in $\widetilde{\mathbf{W}}^N$

$$\begin{aligned} &\mathbf{W} - \mathbf{P}^{\mathrm{N}} \mathbf{G}_{\mathrm{E}}^{\mathrm{m}} \frac{b}{a} \mathbf{W} = \mathbf{W}^0, \\ &\mathbf{W}^0 = \mathbf{P}^{\mathrm{N}} \sqrt{\mathbf{Re}\, \sigma_b} \mathbf{E}^N. \end{aligned} \tag{9}$$

Since $\frac{b}{a} < 1$, $\mathbf{G}_{\mathrm{E}}^{\mathrm{m}}$ is a contracting operator and $\left\|\mathbf{P}^{\mathrm{N}}\right\| = 1$, it can be easily shown that (9) has a unique solution $\mathbf{W}$ in $\widetilde{\mathbf{W}}^N$, Kruglyakov (2011); Singer (2008). Moreover, $\mathbf{W}$ approximates $\mathbf{E}$ with the first order of d in $\mathbf{L}_2[\Omega]$, where $d = \max\limits_{n=1\dots N} d_n$, d_n is a diameter of the subdomain Ω_n, Kruglyakov (2011).

Using the definition of $\widetilde{\mathbf{W}}^N$ the components of $\mathbf{W} = (W_x, W_y, W_z)$ can be expressed as

$$W_\gamma = \sum_{k=1}^{N} U_n^\gamma W_n, \quad \gamma = x, y, z. \tag{10}$$

Using (8) to (10) and taking into account that σ_a, σ_b are piecewise functions, one obtains the following system of linear equations for the coefficients $\mathbf{U}_n = (U_n^x, U_n^y, U_n^z)$, $n = 1 \dots N$

$$\mathbf{U}_n - \sum_{m=1}^{N} \hat{\gamma}^m \widehat{K}_n^m \mathbf{U}_m = \mathbf{U}_n^0, \tag{11}$$

where

$$\begin{aligned}
\widehat{K}_n^m &= \hat{I} + \frac{2}{V_n}\sqrt{\mathbf{Re}\,\sigma_b^m\,\mathbf{Re}\,\sigma_b^n}\,\hat{B}_n^m,\\
\widehat{B}_n^m &= \int\limits_{\Omega_n}\int\limits_{\Omega_m} \widehat{G}^E(M,M_0)d\Omega_{M_0}d\Omega_M,\\
\hat{\gamma}^m &= \frac{\sigma_a^m - \sigma_b^m}{\sigma_a^m + \overline{\sigma_b^m}},\\
\mathbf{U}_n^0 &= \frac{\sqrt{\mathbf{Re}\,\sigma_b^n}}{V_n}\int\limits_{\Omega_n}\mathbf{E}^N(M)d\Omega_M.
\end{aligned} \tag{12}$$

Note that $\widehat{K}_n^m$, $\widehat{B}_n^m$, $\hat{I}$, $\hat{\gamma}^m$ are 3×3 matrices, $\hat{I}$ is an identity matrix, $\hat{\gamma}^m$ is a diagonal matrix. The system (11) has a unique solution, Kruglyakov (2011); Singer (2008).

Using the solution $\mathbf{U}_n$ of system (11) one can approximate $\widetilde{\mathbf{E}}(M)$ and $\widetilde{\mathbf{H}}(M)$ for any point $M \in R^3$ with

$$\begin{aligned}
\mathbf{E}(M) \approx \widetilde{\mathbf{E}}(M) &= \mathbf{E}^N(M) + \sum_{n=1}^{N}(\sigma_a^n - \sigma_b^n)\,\mathbf{U}_n\int\limits_{\Omega_n}\widehat{G}^E(M,M_0)d\Omega_{M_0},\\
\mathbf{H}(M) \approx \widetilde{\mathbf{H}}(M) &= \mathbf{E}^H(M) + \sum_{n=1}^{N}(\sigma_a^n - \sigma_b^n)\,\mathbf{U}_n\int\limits_{\Omega_n}\widehat{G}^H(M,M_0)d\Omega_{M_0}.
\end{aligned} \tag{13}$$

Relations (13) are first order approximations of d in $\mathbf{C}$ for $M \notin \Omega$, Kruglyakov (2011), and result in fast and relatively simple computations. The main challenge is to calculate matrix coefficients and solve the system (11).

3 Computational Challenges

3.1 Memory Requirements

The main challenge of the integral equation approach is in solving of the system of linear equations with dense matrices (11). The storage of these matrices in RAM is

also problematic. The standard approach, Avdeev et al (1997), is to use the property

$$\widehat{G}^E(M,M_0) = \widehat{G}^E(x-x_0, y-y_0, z, z_0). \tag{14}$$

For the implementation purposes consider now $\Omega \subset R^3$ to be a rectangular domain. As before Ω is divided in $N = N_x N_y N_z$ rectangular subdomains Ω_n, $n = 1,\dots,N$, where N_x, N_y, N_z are the number of subdomains in X, Y, Z directions respectively. Suppose also that each Ω_n has the same size $h_x \times h_y$ in XY plane. Then

$$\widehat{B}_n^m = \int\limits_{\Omega_n}\int\limits_{\Omega_m} \widehat{G}^E(M,M_0)\, d\Omega_{M_0} d\Omega_M = \widehat{B}_n^m\left(I_x^n - I_x^m, I_y^n - I_y^m, I_z^n, I_z^m\right), \tag{15}$$

where $I_x^n, I_x^m \in \{1,2,\dots N_x\}$, $I_y^n, I_y^m \in \{1,2,\dots N_y\}$, $I_z^n, I_z^m \in \{1,2,\dots N_z\}$, $n,m = 1\dots N$. Therefore $\widehat{B}_n^m$ is a block Toeplitz matrix induced by the block vector $(C^y_{-(N_y-1)}$, $C^y_{-(N_y-2)}, \dots, C^y_{N_y-2}, C^y_{N_y-1})$. Each block C_i^y, $i = -(N_y-1)\dots N_y - 1$ is also a block Toeplitz matrix and is induced by the block vector $(D^i_{-(N_x-1)}, D^i_{-(N_x-2)}, \dots D^i_{N_x-2}, D^i_{N_x-1})$. The D_j^i is a 3×3 block matrix with the structure

$$D_j^i = Q(i,j) = \begin{pmatrix} Q_{xx} & Q_{xy} & Q_{xz} \\ Q_{yx} & Q_{yy} & Q_{yz} \\ Q_{zx} & Q_{zy} & Q_{zz} \end{pmatrix}. \tag{16}$$

Here $Q_{\alpha\beta}$ are the matrices of the order N_z, $\alpha,\beta = x,y,z$, $i = -(N_y-1)\dots N_y - 1$, $j = -(N_x-1)\dots N_x - 1$.

Let A be a matrix corresponding to the system of linear equations (11). Then

$$A = S + R_1 B R_2, \tag{17}$$

where S, R_1, R_2 are the diagonal matrices; $B = \left\{\widehat{B}_n^m\right\}$ is the block Toeplitz matrix described above.

In view of (17) it follows that only $36 \cdot N_x N_y N_z^2 \cdot 16 + O(N_x N_y N_z)$ bytes are required to store matrix A in double precision. Using the equivalence $G^E_{xy} = G^E_{yx}$ this requirement can be reduced to $32 \cdot N_x N_y N_z^2 \cdot 16 + O(N_x N_y N_z)$ bytes as in Avdeev et al (1997). This memory requirement can be reduced in 8 times by virtue of the following Lemmas.

Lemma 1 *If $\widehat{G}^E(M, M_0)$ is an electrical Green's tensor of any layered media, then it possesses symmetric and antisymmetric properties in Cartesian coordinates along the vertical dimension*

$$
\begin{aligned}
G^E_{xx}(x-x_0, y-y_0, z, z_0) &= G^E_{xx}(x-x_0, y-y_0, z_0, z), \\
G^E_{yy}(x-x_0, y-y_0, z, z_0) &= G^E_{yy}(x-x_0, y-y_0, z_0, z), \\
G^E_{zz}(x-x_0, y-y_0, z, z_0) &= G^E_{zz}(x-x_0, y-y_0, z_0, z), \\
G^E_{xy}(x-x_0, y-y_0, z, z_0) &= G^E_{yx}(x-x_0, y-y_0, z, z_0), \\
G^E_{xy}(x-x_0, y-y_0, z, z_0) &= G^E_{xy}(x-x_0, y-y_0, z_0, z), \\
G^E_{zx}(x-x_0, y-y_0, z, z_0) &= -G^E_{xz}(x-x_0, y-y_0, z_0, z), \\
G^E_{zy}(x-x_0, y-y_0, z, z_0) &= -G^E_{yz}(x-x_0, y-y_0, z_0, z).
\end{aligned}
\tag{18}
$$

Lemma 2 *If $\widehat{G}^E(M, M_0)$ is an electrical Green's tensor of any layered media, then it possesses symmetric and antisymmetric properties in Cartesian coordinates along*

the lateral dimensions

$$
\begin{gathered}
G^E_{\alpha\alpha}(x-x_0,y-y_0,z,z_0) = G^E_{\alpha\alpha}(x_0-x,y-y_0,z,z_0) = \\
G^E_{\alpha\alpha}(x-x_0,y_0-y,z,z_0) = G^E_{\alpha\alpha}(x_0-x,y_0-y,z,z_0), \\
G^E_{xy}(x-x_0,y-y_0,z,z_0) = -G^E_{xy}(x_0-x,y-y_0,z,z_0) = \\
-G^E_{xy}(x-x_0,y_0-y,z,z_0) = G^E_{xy}(x_0-x,y_0-y,z,z_0), \\
G^E_{zx}(x-x_0,y-y_0,z,z_0) = -G^E_{zx}(x_0-x,y-y_0,z,z_0) = \\
G^E_{zx}(x-x_0,y_0-y,z,z_0) = -G^E_{zx}(x_0-x,y_0-y,z,z_0), \\
G^E_{zy}(x-x_0,y-y_0,z,z_0) = G^E_{zy}(x_0-x,y-y_0,z,z_0) = \\
-G^E_{zy}(x-x_0,y_0-y,z,z_0) = -G^E_{zy}(x_0-x,y_0-y,z,z_0), \\
\alpha \in \{x,y,z\}.
\end{gathered}
\tag{19}
$$

These lemmas are trivial corollaries from Lorentz reciprocity, Ward and Hohmann (1988) and Eq. (14). From relations (15) and (18) it follows

$$
\begin{gathered}
Q_{zx} = -Q^T_{xz}, Q_{zy} = -Q^T_{yz}, \\
Q_{xx} = Q^T_{xx}, Q_{yy} = Q^T_{yy}, Q_{zz} = Q^T_{zz}, \\
Q_{xy} = Q^T_{xy} = Q_{yx} = Q^T_{yx},
\end{gathered}
\tag{20}
$$

where ^{T} indicates a matrix transpose.

Therefore, one needs to store only Q_{xz}, Q_{yz} and upper diagonal parts of Q_{xx}, Q_{xy}, Q_{yy}, Q_{zz}. Moreover the values $Q(i,j)$ can be stored only for $i = 0,\dots,N_y-1, j = 0,\dots,N_x-1$, since (19) allows to obtain these values for negative i or j from suitable symmetric/antisymmetric properties.

Thus only $2\cdot N_xN_yN_z\cdot(2N_z+1)\cdot 16$ bytes are required to store $\widehat{B}^m_n$ which is 8 times less than the memory requirements in Avdeev et al (1997, 2002); Hursan and Zhdanov

(2002). It is worth to stress again, that this is valid for any background layered media and without the conditions on the subdomains to be of the same vertical sizes.

3.2 Matrix Coefficients Computation

The next computational challenge of the Galerkin approach is the evaluation of the coefficients $\widehat{B}_n^m$, $n,m = 1\ldots N$, that is the double volumetric integrals of the $\widehat{G}^E$ in the RHS of (15), with desired accuracy. The components of $\widehat{G}^E$ are the improper integrals containing the Bessel functions, Appendix A. The integration in vertical direction is performed analytically using the fundamental function of layered media approach from Dmitriev et al (2002), Appendix B. The main problem, however, is the integration over the horizontal domains. In this case one needs to compute the fifth-order integrals over the fast-oscillating functions.

The integrals in (15) are double volumetric ones, thus they have only weak singularity. Therefore, one can change the order of integration and make an appropriate substitution and convert the fifth-order integral to a convolution with the specific kernel. Following the standard approach of convolution calculation the spectrum of this kernel is computed and the digital filter is constructed, Appendix C.

It is important to emphasize that both the knots and the weights in the obtained filter significantly depend on the integration domains. On the contrary, the integration over different horizontal domains is completely data independent. This is used in parallel algorithm.

The computational experiments demonstrate (Sect. 4) that the used filters provide suitable accuracy even for the models with high conductivity contrast.

3.3 Parallel Implementation

The most essential part of any iterative method for solving a system of linear equations is the matrix-vector multiplication. Since matrix B is a block Toeplitz matrix, one can use the two-dimensional Fast Fourier Transform (FFT) to speed up this operation, Avdeev et al (1997). Therefore, instead of matrices $Q(i,j)$ the discrete Fourier transformations $\widetilde{Q}(i,j)$ are stored. This requires the same amount of memory since the discrete Fourier transform preserves the symmetricity/antisymmetricity of data.

The multiplication of block Toeplitz matrix B on some vector $\mathbf{V} \in \widetilde{\mathbf{W}}^N$ is performed via the following three-step algorithm:

1. Compute $3N_z$ forward FFT of vector $\mathbf{V}$;
2. Compute $36N_xN_y$ algebraic matrix-vector multiplications of order N_z to obtain vector $\tilde{\mathbf{V}}$;
3. Compute $3N_z$ backward FFT of vector $\tilde{\mathbf{V}}$.

The multiplications in Step 2 are further divided into $4N_xN_y$ groups which are mutually data independent. This allows to implement the special scheme of distributed data storage and a parallel algorithm of IE solver, described below.

For simplicity, consider $2N_y$ nodes and assume that Nx is even. The distributed storage of matrix is organized in a special way: the half of block-vector $\widetilde{Q}(n,j)$, $j = 0 \ldots N_x/2-1$ is stored at nth node, $n = 0 \ldots N_y - 1$, while $\widetilde{Q}(n,j)$, $j = N_2/2 \ldots N_x$ is stored at node $n+N_y$, $n = 0 \ldots N_y - 1$, Table 1.

This storage organization is used to develop the solver with suitable features of parallelization:

(i) The coefficients of matrices B, S, R_1, R_2 stored at different nodes are computed simultaneously and completely data independent;

(ii) The iterative method is executed using the distributed FGMRES implementation by Fraysse et al (2003);

(iii) The distributed two-dimensional Fourier transform is computed via the author's implementation using FFTW3 library for local FFT transforms;

(iv) The calculation of the local algebraic matrix-vector multiplication is processed by using OpenBlas library;

(v) For all the stages of the computational process the hybrid MPI+OpenMP scheme is used.

To demonstrate the scalability of the implemented parallelization the COMMEMI3D-3 model is used with $N_x = 176$, $N_y = 224$, $N_z = 118$, that is with cubic subdomains with 25 m edges, Sect. 4. The computational experiments performed at "Bluegene/P", HPC "Lomonosov" (MSU) and Piz Daint (Swiss National Supercomputing Center) showed good speed increment depending on the number of processes (Fig. 2). Matrix calculation time includes time of FFT calculation of $\widehat{B}_n^m$. The solid black line means ideal linear speed up. Note, that for such high-contrast model matrix calculation time (crosses) is small enough compared to solving of the system of linear equations (circles). One can see that the scalability is close to a linear.

4 High Conductivity Contrast Modeling

The accurate computation of the EM field in a high conductivity contrast media is one of the most complex problems of EM modeling due to strong codependency

between conductivity contrast and matrix condition number, Pankratov et al (1995); Pankratov and Kuvshinov (2016); Singer (1995). The conductivity contrast means the ratio between the real parts of anomalous conductivity $\mathbf{Re}\,\sigma_a(M)$ and background conductivity $\mathbf{Re}\,\sigma_b(M)$ at the same point M.

The high conductivity contrast COMMEMI3D-3 model, Hursan and Zhdanov (2002); Varentsov et al (2000), is used as one of the test models for the presented solver. This model schematically describes the conductivity distribution typical for the ore exploration by the audio-magnetotelluric sounding. Following magnetotelluric (i.e., low-frequency) sounding tradition in the rest of this section the conductivity is a real-valued function.

The COMMEMI3D-3 model consists of seven rectangular blocks placed in a layered media and oriented along coordinate axes. Their conductivities σ (in S/m) and positions (coordinates of the opposite corners in km) are listed in Table 2 and depicted in Fig. 3. The layered background of the model consists of the upper halfspace $z<0$ (air) with conductivity of 0 S/m, two layers with the conductivity of 10^{-3}, 10^{-4} S/m, and a lower halfspace with conductvity of 0.1 S/m. The thickness of the first and the second layers is 1 and 6.5 km respectively. One can see that maximum conductivity contrast is 10^4 in the first layer and $3.3\cdot 10^4$ in the second one.

The modeling of magnetotelluric sounding was performed for various discretizations (cubic subdomains of different sizes) and periods $T=2\pi/\omega$, and was compared with the results from modern FE solver by Grayver and Kolev (2015). Figures 4 and 5 represent, correspondingly, the apparent resistivities ρ_{xy} at profile $x=1.9$ km and ρ_{yx} at profile $y=3.83$ km for the period 1 s. One can see that the agreement with FE

(magenta circles) is good even for rather coarse anomaly discretization (black curve). The exception is the area $[3.5, 4.5]$ km on the profile $y = 3.83$ km (Fig. 5) above the high-conductivity block. This is amended by taking finer discretization (azure curve).

Figure 6 shows the apparent conductivity ρ_{yx} at site $(3.975, 3.83)$ km, that is above the high-conductivity block, at different periods. One can see that the finer discretization is needed only for the periods $\left[10^{-1}, 10^{1}\right]$ s. The reason behind this effect is the drastic change in the electric field inside of the compact high-conductivity block that does not allow to use the piecewise approximation on coarse discretization. The solver by Grayver and Kolev (2015) uses the second order polynomials which are very effective in such situations. At the same time, the coarse discretization can be efficiently used for smaller and larger periods. It is worth emphasizing that this concerns only the area above the high-conductivity block, while at the point $(1.9, 1.7)$ km, Fig. 7 shows good correspondence for all periods.

Figures 8 to 11 demonstrate area distribution of the apparent conductivity and impedance phases for 1 s period. One can see that the variation in apparent conductivity is of the four order of magnitude with very drastic transition. The phase change of the impedance is 10 degrees, and the transition is again drastic. It is worth reminding, that one of the peculiarities of IE method is quite weak dependence of computational costs on the number of sites where the field is computed. This allowed to obtain the maps with such drastic transitions without the additional computational costs.

5 Conclusion

The presented solver for volumetric integral equations of electrodynamics requires 8 times less amount of RAM compared to the other existing volumetric IE solvers. The high parallelization degree allows the efficient usage of modern HPC systems to perform computations for large scale models (up to 10^9 subdomains) with a complex conductivity distribution.

The good fit with the high-order FE method demonstrates the high accuracy of this solver, including application to the high conductivity contrast problems.

The developed solver named “Gnu Integral Equation Modeling in ElectroMagnetic Geophysics” (GIEM2G) is implemented as hybrid MPI+OpenMP software on modern Fortran language. The GIEM2G is an open source software distributed under the GPLv2 license and can be simple cloned from GitLab by *git -clone git@gitlab.com:m.kruglyakov/GIEM2G.git*.

Acknowledgements The research of the first author was supported by the Russian Foundation for Basic Research (grant no. 13-05-12018-OFI_M). As a visiting fellow in ETH Zurich he was also partially supported by the Swiss National Science Foundation (grant no. IZK0Z2_163494) and ETH Zurich. Authors acknowledge the teams of HPC CMC Lomonosov MSU for the access to “Bluegene/P” HPC, the Lomonosov MSU Research Computing Center for the access to HPC “Lomonosov” Sadovnichy et al (2013) and the Swiss National Supercomputing Center (CSCS) grant (project ID s577). Authors also would like to thank Alexander Grayver, ETH Zurich, for providing data for comparison and Alexey Kuvshinov, ETH Zurich, for suggestions and helpful discussions.

References

Anderson W (1979) Numerical integration of related hankel transforms of order 0 and 1 by adaptive digital filtering. Geophysics 44:1287–1305

Avdeev D, Knizhnik S (2009) 3D integral equation modeling with a linear dependence on dimensions. Geophysics 74:89–94

Avdeev D, Kuvshinov A, Pankratov O, Newman G (2002) Three-dimensional induction logging problems, Part I: An integral equation solution and model comparisons. Geophysics 67(2):413–426

Avdeev DB, Kuvshinov AV, Pankratov OV, Newman GA (1997) High-performance three-dimensional electromagnetic modelling using modified neumann series. wide-band numerical solution and examples. J Geomagn Geoelectr 49:1519–1539

Börner RU (2010) Numerical modelling in geo-electromagnetics: advances and challenges. Surv Geophys 31:225–245

Chave A, Jones A (2012) The Magnetotelluric Method: Theory and Practice. Cambridge Univ. Press

Delves LM, Mohamed JL (1985) Computational Methods for Integral Equations. Cambridge University Press

Dmitriev V, Silkin A, Farzan R (2002) Tensor Green function for the system of Maxwell's equations in a layered medium. Comput Math and Modeling 13(2):107–118

Ernst O, Gander M (2012) Why it is difficult to solve helmholtz problems with classical iterative methods. In: Graham IG, Hou TY, Lakkis O, Scheichl R (eds) Numerical Analysis of Multiscale Problems, Lecture Notes in Computational Science

and Engineering, vol 83, Springer Berlin Heidelberg, pp 325–363

Fraysse V, Giraud L, Gratton S, Langou J (2003) A set of GMRES routines for real and complex arithmetics on high performance computers. URL http://www.cerfacs.fr/algor/reports/2003/TR_PA_03_03.pdf

Grayver A, Kolev T (2015) Large-scale 3d geo-electromagnetic modeling using parallel adaptive high-order finite element method. Geophysics 80(6):277–291

Hursan G, Zhdanov MS (2002) Contraction integral equation method in three-dimensional electromagnetic modeling. Radio Science 37(6):1–1–1–13, DOI 10.1029/2001RS002513, URL http://dx.doi.org/10.1029/2001RS002513, 1089

Kamm J, Pedersen LB (2014) Inversion of airborne tensor vlf data using integral equations. Geophysical Journal International 198(2):775–794, DOI 10.1093/gji/ggu161

Koyama T, Utada H, Avdeev D (2008) Fast and memory-saved 3-D forward modeling code for MT by using integral equation method. In: Abstract book, 19th workshop on electromagnetic induction in the Earth, China

Kruglyakov M (2011) Modified integral current methods in electrodynamics of non-homogeneous media. Comput Math and Modeling 22(3):246–254

Mulder W (2006) A multigrid solver for 3D electromagnetic diffusion. Geophys Prospect 54:633–649

Pankratov O, Kuvshinov A (2016) Applied mathematics in em studies with special emphasis on an uncertainty quantification and 3-d integral equation modelling. Surveys in Geophysics 37(1):109–147, DOI 10.1007/s10712-015-9340-4, URL

http://dx.doi.org/10.1007/s10712-015-9340-4

Pankratov O, Avdeyev D, Kuvshinov A (1995) Electromagnetic-field scattering in a heterogeneous Earth: A solution to the forward problem. Izv-Phys Solid Eart+ 31(3):201–209

Raiche AP (1974) An integral equation approach to three-dimensional modelling. Geophys J Int 36(2):363–376

Saad Y (1993) A flexible inner-outer preconditioned gmres algorithm. SIAM J Sci Comput 14(2):461–469

Sadovnichy V, Tikhonravov A, Voevodin V, Opanasenko V (2013) "Lomonosov": Supercomputing at Moscow State University. In: Contemporary High Performance Computing: From Petascale toward Exascale, Boca Raton, United States, Chapman & Hall/CRC Computational Science, pp 283–307

Singer B (1995) Method for solution of Maxwell's equations in non-uniform media. Geophys J Int 120:590–598

Singer B (2008) Electromagnetic integral equation approach based on contraction operator and solution optimization in Krylov subspace. Geophys J Int 175:857–884

Sun J, Kuvshinov A (2015) Accelerating em integral equation forward solver for global geomagnetic induction using svd based matrix compression method. Geophys J Int 200(2):1005–1011

Varentsov IM, Fomenko IY, Golubev NG, Mehanee S, Hursan G, Zhdanov MS (2000) Comparative study of 3-D finite difference and integral equation methods. In: Proceedings of 2000 Consortium for Electomagnetic Modeling and Inversion Annual

Meeting, University of Utah, Salt Lake City, pp 35–74

Wannmaker PE (1991) Advances in three-dimensional magnetotelluric modeling using integral equations. Geophysics 56:1716–1728

Ward SH, Hohmann GW (1988) 4. Electromagnetic Theory for Geophysical Applications, chap 4, pp 130–311

Weidelt P (1975) Electromagnetic induction in three-dimensional structures. J Geophys-Z Geophys 41:85–109

Appendix A: Green's Tensor

Following the notations from Dmitriev et al (2002), the electrical $\widehat{G}^E$ and magnetic $\widehat{G}^H$ tensors of layered media can be written as

$$\begin{aligned} \widehat{G}^E &= \widehat{G} + \operatorname{grad}\left(\frac{\mu_0}{k^2}\operatorname{div}\frac{\widehat{G}}{\mu_0}\right), \\ \widehat{G}^H &= \frac{1}{i\omega\mu_0}\operatorname{curl}\widehat{G}, \\ k^2 &= i\omega\mu_0\sigma_b, \end{aligned} \tag{21}$$

where

$$\widehat{G}(M,M_0) = \begin{pmatrix} G_1(M,M_0) & 0 & 0 \\ 0 & G_1(M,M_0) & 0 \\ \frac{\partial g(M,M_0)}{\partial x} & \frac{\partial g(M,M_0)}{\partial y} & G_2(M,M_0) \end{pmatrix} \tag{22}$$

and

$$G_1(M,M_0) = \frac{i\omega\mu_0}{4\pi}\int\limits_0^\infty J_0(\lambda\rho)U_1(\lambda,z,z_0)\lambda d\lambda,$$
$$G_2(M,M_0) = \frac{i\omega\mu_0}{4\pi}\int\limits_0^\infty J_0(\lambda\rho)U_\sigma(\lambda,z,z_0)\lambda d\lambda,$$
$$g(M,M_0) = \frac{i\omega\mu_0}{4\pi}\int\limits_0^\infty J_0(\lambda\rho)\left(\frac{\partial}{\partial z_0}U_\sigma(\lambda,z,z_0) - \frac{\partial}{\partial z}U_1(\lambda,z,z_0)\right)\frac{d\lambda}{\lambda},$$
$$M = M(x,y,z) \quad M_0 = M_0(x_0,y_0,z_0) \quad \rho = \sqrt{(x-x_0)^2+(y-y_0)^2}. \tag{23}$$

Here J_0 is a zero-order Bessel function of the first kind, and functions $U_\gamma(\lambda,z,z_0)$, $\gamma = 1,\sigma$ are the fundamental functions of the layered media (Appendix B).

From (21) and (22) one gets

$$\widehat{G}^E = \begin{Bmatrix} G_1 + \frac{1}{k^2}\frac{\partial^2}{\partial x^2}\left(G_1 + \frac{\partial g}{\partial z}\right) & \frac{1}{k^2}\frac{\partial^2}{\partial x\partial y}\left(G_1 + \frac{\partial g}{\partial z}\right) & \frac{1}{k^2}\frac{\partial^2 G_2}{\partial x\partial z} \\ \frac{1}{k^2}\frac{\partial^2}{\partial x\partial y}\left(G_1 + \frac{\partial g}{\partial z}\right) & G_1 + \frac{1}{k^2}\frac{\partial^2}{\partial y^2}\left(G_1 + \frac{\partial g}{\partial z}\right) & \frac{1}{k^2}\frac{\partial^2 G_2}{\partial y\partial z} \\ \frac{\partial g}{\partial x} + \frac{1}{k^2}\frac{\partial^2}{\partial x\partial z}\left(G_1 + \frac{\partial g}{\partial z}\right) & \frac{\partial g}{\partial y} + \frac{1}{k^2}\frac{\partial^2}{\partial y\partial z}\left(G_1 + \frac{\partial g}{\partial z}\right) & G_2 + \frac{1}{k^2}\frac{\partial^2 G_2}{\partial z^2} \end{Bmatrix}. \tag{24}$$

Note, that $G^E_{xz}(M,M_0) = -G^E_{zx}(M_0,M)$, $G^E_{yz}(M,M_0) = -G^E_{zy}(M_0,M)$ according to Lorentz reciprocity.

Let $\Omega_n = S_n \times [z_n^1, z_n^2]$, $\Omega_m = S_m \times [z_m^1, z_m^2]$, where S_n, S_m are horizontal rectangular domains, and let $\sigma_b = \sigma_b^n$ inside $[z_n^1, z_n^2]$, $\sigma_b = \sigma_b^m$ inside $[z_m^1, z_m^2]$. That is the subdomains do not intersect the boundaries of the layers. Taking into account (12), (21) and (24) one can see that $\widehat{B}_n^m$ is expressed in terms of double volumetric integrals with weak integrable singularity, so the order of integration can be changed. Then

using (23) and (24) one obtains

$$\widehat{B}_n^m = \frac{1}{4\pi}\begin{Bmatrix} I_1^{n,m}+I_{xx}^{n,m} & I_{xy}^{n,m} & I_x^{n,m} \\ I_{xy}^{n,m} & I_1^{n,m}+I_{yy}^{n,m} & I_y^{n,m} \\ -I_x^{m,n} & -I_y^{m,n} & I_2^{n,m}+I_{zz}^{n,m} \end{Bmatrix}, \tag{25}$$

where

$$\begin{aligned}
I_1^{n,m} &= \int\limits_{S_n}\int\limits_{S_m}\left(\int\limits_0^\infty J_0(\lambda\rho)V_1^{n,m}(\lambda)\lambda d\lambda\right)dx_0dy_0dxdy,\\
I_2^{n,m} &= \int\limits_{S_n}\int\limits_{S_m}\left(\int\limits_0^\infty J_0(\lambda\rho)V_2^{n,m}(\lambda)\lambda d\lambda\right)dx_0dy_0dxdy,\\
I_{\alpha\beta}^{n,m} &= \int\limits_{S_n}\frac{\partial^2}{\partial\alpha\partial\beta}\left\{\int\limits_{S_m}\left(\int\limits_0^\infty J_0(\lambda\rho)\left[V_1^{n,m}(\lambda)+V_3^{n,m}(\lambda)\right]\frac{d\lambda}{\lambda}\right)dx_0dy_0\right\}dxdy,\\
I_\alpha^{n,m} &= \int\limits_{S_n}\frac{\partial}{\partial\alpha}\left\{\int\limits_{S_m}\left(\int\limits_0^\infty J_0(\lambda\rho)V_4^{n,m}(\lambda)\lambda d\lambda\right)dx_0dy_0\right\}dxdy,\\
I_{zz}^{n,m} &= \int\limits_{S_n}\int\limits_{S_m}\left(\int\limits_0^\infty J_0(\lambda\rho)V_5^{n,m}(\lambda)\lambda d\lambda\right)dx_0dy_0dxdy.
\end{aligned} \tag{26}$$

Here $\alpha = x, y$, $\beta = x, y$, and

$$V_1^{n,m}(\lambda) = i\omega\mu_0 \int_{z_n^1}^{z_n^2}\int_{z_m^1}^{z_m^2} U_1(\lambda, z, z_*)dz_*dz,$$

$$V_2^{n,m}(\lambda) = i\omega\mu_0 \int_{z_n^1}^{z_n^2}\int_{z_m^1}^{z_m^2} U_\sigma(\lambda, z, z_*)dz_*dz,$$

$$V_3^{n,m}(\lambda) = \frac{1}{\sigma_b^n}\int_{z_n^1}^{z_n^2}\frac{\partial}{\partial z}\left(\int_{z_m^1}^{z_m^2}\left[\frac{\partial}{\partial z_*}U_\sigma(\lambda, z, z_*)\right]dz_*\right)dz,$$

$$V_4^{n,m}(\lambda) = \frac{1}{\sigma_b^n}\int_{z_n^1}^{z_n^2}\frac{\partial}{\partial z}\left(\int_{z_m^1}^{z_m^2} U_\sigma(\lambda, z, z_*)dz_*\right)dz,$$

$$V_5^{n,m}(\lambda) = \frac{1}{\sigma_b^n}\int_{z_n^1}^{z_n^2}\frac{\partial^2}{\partial z^2}\left(\int_{z_m^1}^{z_m^2} U_\sigma(\lambda, z, z_*)dz_*\right)dz. \quad (27)$$

Therefore, to obtain the coefficients of $\hat{B}_n^m$ one needs computational methods to find "horizontal" integrals (26) and "vertical" integrals (27). These methods are presented in the next sections.

Appendix B: Vertical Integration

The integrals in (27) are expressed in terms of the so-called fundamental function of the layered media, Dmitriev et al (2002). Consider the media with $N_{lay} - 1$ homogenous layers with complex conductivities σ_n, $n = 1 \ldots N_{lay} - 1$, the upper halfspace (air, the zeroth layer) with complex conductivity σ_0 and the lower halfspace (the N_{lay}-th layer) with conductivity $\sigma_{N_{lay}}$. Note, that in EM sounding problems typically $\mathbf{Re}\,\sigma_0 \leq 10^{-9}$.

The function $U_\gamma(z,z_*,\lambda)$ is defined as a unique solution of the problem

$$\begin{cases} \dfrac{\partial^2}{\partial z^2}U_\gamma(z,z_*,\lambda)-\eta_0^2U_\gamma(z,z_*,\lambda)=0, z<d_1, z\neq z_*, \\ \dfrac{\partial^2}{\partial z^2}U_\gamma(z,z_*,\lambda)-\eta_n^2U_\gamma(z,z_*,\lambda)=0, d_n<z<d_{n+1}, z\neq z_*, \\ \dfrac{\partial^2}{\partial z^2}U_\gamma(z,z_*,\lambda)-\eta_{N_{lay}}^2U_\gamma(z,z_*,\lambda)=0, z>d_{N_{lay}}, z\neq z_*, \\ \left[U_\gamma(z,z_*,\lambda)\right]_{z=d_n}=0, \\ \left[\dfrac{1}{\gamma}\dfrac{\partial}{\partial z}U_\gamma(z,z_*,\lambda)\right]_{z=d_n}=0, \\ \left[U_\gamma(z,z_*,\lambda)\right]_{z=z_*}=0, \\ \left[\dfrac{\partial}{\partial z}U_\gamma(z,z_*,\lambda)\right]_{z=z_*}=-2, \\ \left|U_\gamma(z,z_*,\lambda)\right|\to 0 \text{ as } z\to\pm\infty, \\ \eta_m^2=\lambda^2-k_m^2, \quad k_m^2=i\omega\mu_0\sigma_m, \\ m=0\ldots N_{lay}, \quad n=1\ldots N_{lay}-1, \quad 0<\lambda<\infty. \end{cases} \tag{28}$$

The following procedure is performed to obtain an explicit expression for U_γ that allows analytical integration. Let $l_0=0$, $l_{N_{lay}}=0$, $l_n=d_{n+1}-d_n$, $n=1\ldots N_{lay}-1$.

Define p_m^γ, q_m^γ, $m = 0 \ldots N_{lay}$ by the recurrent expressions

$$
\begin{aligned}
&p_0^\gamma = 0; && q_{N_{lay}}^\gamma = 0;\\
&p_1^\gamma = \frac{1-\alpha_0^\gamma \frac{\eta_0}{\eta_1}}{1+\alpha_0^\gamma \frac{\eta_0}{\eta_1}}; && q_{N_{lay}-1}^\gamma = \frac{1-\beta_{N_{lay}}^\gamma \frac{\eta_{N_{lay}}}{\eta_{N_{lay}-1}}}{1+\beta_{N_{lay}}^\gamma \frac{\eta_{N_{lay}}}{\eta_{N_{lay}-1}}};\\
&p_{m+1}^\gamma = \frac{1+\alpha_m^\gamma \frac{\eta_m}{\eta_{m+1}} \frac{p_m^\gamma e^{-2\eta_m l_m}-1}{p_m^\gamma e^{-2\eta_m l_m}+1}}{1-\alpha_m^\gamma \frac{\eta_m}{\eta_{m+1}} \frac{p_m^\gamma e^{-2\eta_m l_m}-1}{p_m^\gamma e^{-2\eta_m l_m}+1}}, && q_{m-1}^\gamma = \frac{1+\beta_m^\gamma \frac{\eta_m}{\eta_{m-1}} \frac{q_m^\gamma e^{-2\eta_m l_m}-1}{q_m^\gamma e^{-2\eta_m l_m}+1}}{1-\beta_m^\gamma \frac{\eta_m}{\eta_{m-1}} \frac{q_m^\gamma e^{-2\eta_m l_m}-1}{q_m^\gamma e^{-2\eta_m l_m}+1}},\\
&\quad m \neq N_{lay}; && \quad m \neq 0;\\
&\alpha_m^\gamma = \begin{cases} 1, \gamma = 1; \\ \frac{\sigma_{m+1}}{\sigma_m}, \gamma = \sigma; \end{cases} && \beta_m^\gamma = \begin{cases} 1, \gamma = 1; \\ \frac{\sigma_{m-1}}{\sigma_m}, \gamma = \sigma. \end{cases}
\end{aligned}
\tag{29}
$$

Let $d_0 = d_1$, $d_{N_{lay+1}} = d_{N_{lay}}$ and let points z_r, z_s belong to r and s layers respectively, $0 \le r,s \le N_{lay}$. Then using (29) one gets

$$
U_\gamma(z_r, z_s, \lambda) = \begin{cases} A_{r,s}^\gamma \left(p_r^\gamma e^{2\eta_r d_r} e^{-\eta_r z_r} + e^{\eta_r z_r}\right)\left(e^{-\eta_s z_s} + q_s^\gamma e^{-2\eta_s d_{s+1}} e^{\eta_s z_s}\right) \\ \qquad\qquad \text{for} \quad z_r \le z_s; \\ A_{s,r}^\gamma \left(p_s^\gamma e^{2\eta_s d_s} e^{-\eta_s z_s} + e^{\eta_s z_s}\right)\left(e^{-\eta_r z_r} + q_r^\gamma e^{-2\eta_r d_{r+1}} e^{\eta_r z_r}\right) \\ \qquad\qquad \text{for} \quad z_r > z_s, \end{cases}
\tag{30}
$$

where

$$
\begin{aligned}
&A_{r,s}^\gamma = Q_r^\gamma \times Q_{r+1}^\gamma \times \cdots \times Q_{s-1}^\gamma A_{s,s}^\gamma, \quad \text{for} \quad r < s,\\
&Q_m^\gamma = \frac{1+p_{m+1}^\gamma}{1+p_m^\gamma e^{-2\eta_m l_m}} e^{(\eta_{m+1}-\eta_m)d_{m+1}}, \quad \text{for} \quad m = 1 \ldots N_{lay}-1,\\
&A_{n,n}^\gamma = \frac{1}{\eta_n\left(1-p_n^\gamma q_n^\gamma e^{-2\eta_n l_n}\right)}, \quad \text{for} \quad r = s = n, n = 0 \ldots N_{lay},\\
&A_{r,s}^1 = A_{s,r}^1, \quad A_{r,s}^\sigma = \frac{\sigma_r}{\sigma_s} A_{s,r}^\sigma, \quad \text{for} \quad r > s.
\end{aligned}
\tag{31}
$$

To check (30) one can explicitly substitute (30) in (28) taking into account (29) and (31).

In view of (30) one can see that integrals in (27) (i.e., the integrals over $U_\gamma(z,z_*,\lambda)$ and its partial derivatives) can be integrated analytically with respect to z, z_* over any domains that do not intersect the layer boundaries. However, the rounding errors arising in addition and multiplication of very small or large quantities make the formula (30) impractical for $\lambda \gg 1$. Instead the following formula is used

$$U_\gamma(z_r,z_s,\lambda) = \begin{cases} A^\gamma_{r,s}\left(p^\gamma_r e^{-(\eta_r z_r+\eta_s z_s-2\eta_r d_r)} + q^\gamma_s e^{-(2\eta_s d_{s+1}-(\eta_r z_r+\eta_s z_s))} + \right. \\ \qquad \left. e^{-(\eta_s z_s-\eta_r z_r)} + p^\gamma_r q^\gamma_s e^{-(2(\eta_s d_{s+1}-\eta_r d_r)-(\eta_s z_s-\eta_r z_r))}\right) \\ \qquad\qquad \text{for} \quad z_r \le z_s; \\ A^\gamma_{s,r}\left(p^\gamma_s e^{-(\eta_s z_s+\eta_r z_r-2\eta_s d_s)} + q^\gamma_r e^{-(2\eta_r d_{r+1}-(\eta_s z_s+\eta_r z_r))} + \right. \\ \qquad \left. e^{-(\eta_r z_r-\eta_r z_r)} + p^\gamma_s q^\gamma_r e^{-(2(\eta_r d_{r+1}-\eta_s d_s)-(\eta_r z_r-\eta_s z_s))}\right) \\ \qquad\qquad \text{for} \quad z_r > z_s. \end{cases} \tag{32}$$

Formula (32) overcomes the aforementioned problem, since the real parts of all the exponents powers are negative. The consequent calculations provide accurate and robust results for any $0 < \lambda < \infty$.

Consider N_z subdomains in the discretization in vertical direction. To obtain the matrix $\widehat{B}^m_n$ for the system (15) one needs to compute $O\left(N_z^2\right)$ complex exponents in (32). An algorithm requiring only $O(N_z)$ complex exponents calculations is developed to speed up the integration procedure.

Let $z_0 < z_1 < \cdots < z_{N_z}$. Suppose that the intervals $[z_l, z_{l+1}]$, $l = 0 \ldots N_z - 1$ do not intersect the layers' boundaries. For $i,j = 0 \ldots N_z - 1$, $0 \le \alpha + \beta \le 2$ one needs to calculate $W^{\alpha,\beta}_{i,j}(\gamma) = \int\limits_{z_i}^{z_{i+1}} \frac{\partial^\alpha}{\partial z^\alpha} \left(\int\limits_{z_j}^{z_{j+1}} \left[\frac{\partial^\beta}{\partial z_*^\beta} U_\gamma(z,z_*,\lambda) \right] dz_* \right) dz$.

Let r_l be an index of the layer containing $[z_l, z_{l+1}]$, $l = 0 \ldots N_z - 1$. Then using (30) one obtains for $z_i < z_j$

$$W_{i,j}^{\alpha,\beta}(\gamma) = \int_{z_i}^{z_{i+1}} \left(\frac{\partial^\alpha}{\partial z^\alpha} \int_{z_j}^{z_{j+1}} \left[\frac{\partial^\beta}{\partial z_*^\beta} U_\gamma(z, z_*, \lambda) \right] dz_* \right) dz = H_\gamma^\alpha(z_i, z_{i+1}) \prod_{l=i+1}^{l=j} \Theta_l^\gamma \int_{z_j}^{z_{j+1}} \left(\frac{\partial^\beta}{\partial z_*^\beta} U\gamma(z_j, z_*, \lambda) \right) dz_*, \tag{33}$$

where

$$H_\gamma^\alpha(z_i, z_{i+1}) = \frac{\int_{z_i}^{z_{i+1}} \left(\frac{\partial^\alpha}{\partial z^\alpha} \left[p_{r_i}^\gamma e^{-\eta_{r_i}(z + z_{i+1} - 2d_{r_i})} + e^{-\eta_{r_i}(z_{i+1} - z)} \right] \right) dz}{p_{r_i}^\gamma e^{-2\eta_{r_i}(z_{i+1} - d_{r_i})} + 1},$$

$$\Theta_l^\gamma = \varkappa_l^\gamma \frac{p_{r_l}^\gamma e^{\eta_{r_l}(2d_{r_l} - (z_l + z_{l+1}))} + e^{-\eta_{r_l}(z_{l+1} - z_l)}}{p_{r_l}^\gamma e^{2\eta_{r_l}(d_{r_l} - z_{l+1})} + 1}, \tag{34}$$

$$\varkappa_l^\gamma = \left\{ \begin{array}{c} 1, r_l = r_{l+1} \\ \\ Q_{r_{l+1}}^\gamma, r_l \neq r_{l+1} \end{array} \right\}.$$

All the exponents in (34) vanish as $\lambda \to \infty$, so the corresponding computations do not depend on the round-off errors due to the machine precision. The formulas for $z_i > z_j$ are similar. The integrals $W_{ii}^{\alpha,\beta}$ are computed analytically using (32). Since Θ_l^γ depends only on $l = 1 \ldots N_z$ and $\gamma = 1, \sigma$, one only needs to calculate $O(N_z)$ complex exponents using factorization (33), (34).

Appendix C: Horizontal Integration

The integrals (26) are the particular case of the integral

$$I_{\alpha,\beta} = \int_{S_n} \frac{\partial^{\alpha+\beta}}{\partial x^\alpha \partial y^\beta} \left\{ \int_{S_m} \left[\int_0^\infty J_0(\rho\lambda) f(\lambda) d\lambda \right] dS_m \right\} dS_n, \tag{35}$$

$$\rho = \sqrt{(x - x_0)^2 + (y - y_0)^2}, \quad 0 \leq \alpha + \beta \leq 2,$$

where $f(\lambda)$ is some easily computed function, $S_n = [x_n, x_n + h_x] \times [y_n, y_n + h_y]$, $S_m = [x_m, x_m + h_x] \times [y_m, y_m + h_y]$ are the rectangular domains with similar sizes.

The key feature of the proposed method is transformation of integrals (35) to one-dimensional convolution integral. Taking for simplicity $\alpha = \beta = 0$, one has

$$I_{0,0} = F(R; p, q, \varphi) = \int_0^\infty K(R\lambda; p, q, \varphi) f(\lambda) \frac{d\lambda}{\lambda^4},$$

$$\begin{aligned} K(R\lambda; p, q, \varphi) &= \lambda^4 \int_{S_m} \int_{S_n} J_0(\rho\lambda) dS_m dS_n \\ &= \lambda^4 \int_{x_n}^{x_n+h_x} \int_{y_n}^{y_n+h_y} \int_{x_m}^{x_m+h_x} \int_{y_m}^{y_m+h_y} J_0(\rho\lambda) dx_0 dy_0 dx dy \\ &= \int_0^{R\lambda p} \int_0^{R\lambda q} \int_{R\lambda\left(\cos\varphi - \frac{p}{2}\right)}^{R\lambda\left(\cos\varphi + \frac{p}{2}\right)} \int_{R\lambda\left(\sin\varphi - \frac{q}{2}\right)}^{R\lambda\left(\sin\varphi + \frac{q}{2}\right)} J_0(\tau) d\tilde{x} d\tilde{x}_0 d\tilde{y} d\tilde{y}_0, \end{aligned} \tag{36}$$

where

$$\begin{aligned} &\tau = \sqrt{(\tilde{x} - \tilde{x}_0)^2 + (\tilde{y} - \tilde{y}_0)^2}; \\ &R = \sqrt{\left(x_n - x_m - \frac{h_x}{2}\right)^2 + \left(y_n - y_m - \frac{h_y}{2}\right)^2}; \\ &p = \frac{h_x}{R} \quad q = \frac{h_y}{R} \quad \varphi = \arctan \frac{y_n - y_m - \frac{h_y}{2}}{x_n - x_m - \frac{h_x}{2}}. \end{aligned}$$

Let $\lambda = e^{-t}$, $R = e^s$

$$\begin{aligned} F\left(e^s; p, q, \varphi\right) &= e^{3s} \int_{-\infty}^{\infty} \Phi(s - t; p, q, \varphi) f\left(e^{-t}\right) dt, \\ \Phi(s - t; p, q, \varphi) &= K\left(e^{s-t}; p, q, \varphi\right) e^{-3(s-t)}. \end{aligned} \tag{37}$$

For fixed p, q, φ the integral in (37) is the convolution integral with kernel Φ. Note that for different values of α and β the kernels can be obtained similarly.

The main advantage of using the convolution integrals is that their computation does not require the explicit calculation of kernel Φ. Consider the input function $v(t)$ and the output function $u(s)$ such that

$$u(s) = \int_{-\infty}^{+\infty} \Phi(s-t)v(t)dt. \tag{38}$$

For some $N = 2M$, l, $0 < \xi < 0.5l$, $k = -M \ldots M-1$, define

$$W_s = (-1)^s \frac{1}{N} \sum_{n=-M}^{M-1} \left\{ \frac{\sum_{m=-M}^{M-1} (-1)^m u(ml-\xi) e^{-2i\pi \frac{mn}{N}}}{\sum_{m=-M}^{M-1} (-1)^m v(ml+0.5l) e^{-2i\pi \frac{mn}{N}}} \right\} e^{2i\pi \frac{sn}{N}}. \tag{39}$$

Then for any $g(t)$ one gets

$$\int_{-\infty}^{+\infty} \Phi(s-t)g(t)dt \approx \sum_{s=N_1}^{N_2} W_s g(sl+\xi), \quad -M \le N_1 < N_2 \le M-1. \tag{40}$$

The tradeoff between the accuracy of (40) and the computational time is achieved by the particular selection of M, N_1, N_2, l, ξ and functions u and v.

From (36) and (40) the approximation formulas for (35) can be obtained

$$\begin{aligned} I_{\alpha,\beta} &\approx R^{(3-\alpha-\beta)} \sum_{m=N_1}^{m=N_2} W_m^{\alpha,\beta}(p,q,\varphi,\alpha,\beta) f\left(\frac{\lambda_m}{R}\right), \\ \lambda_m &= e^{ml+\xi}. \end{aligned} \tag{41}$$

For the given input function $v(t) = 8e^{-t^2}\left(t^5 - 4t^3 + 2t\right)$ the output functions for different kernels can be expressed analytically by Gaussian and error functions. Inspired by Anderson (1979) the parameters used are $l = 0.2$, $\xi = 0.0964$, $M = 512$, $N_1 = -250$, $N_2 = 200$. In computational experiments these parameters provided appropriate accuracy in calculation of $\widehat{B}_n^m$.

List of Figures

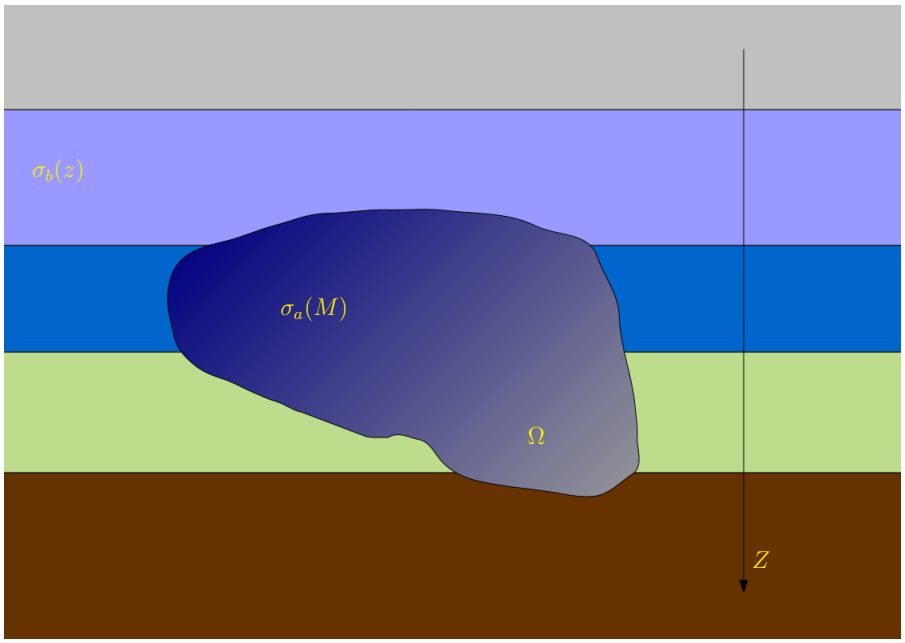

Fig. 1

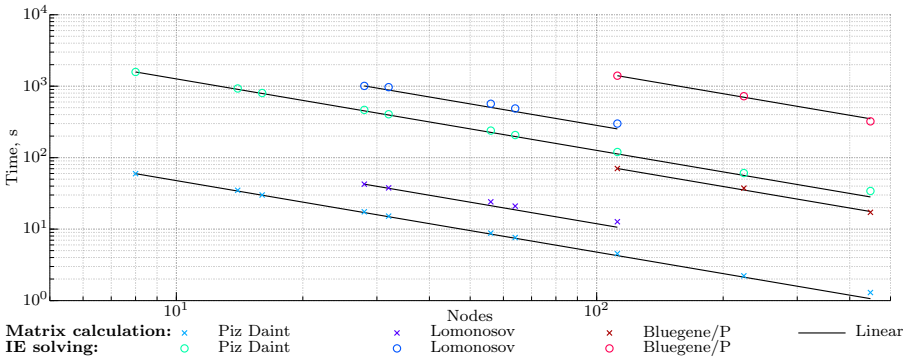
10^4
10^3
10^2
10^1
10^0
Time, s
10^1
10^2
Nodes
Matrix calculation:
IE solving:
Piz Daint
Piz Daint
Lomonosov
Lomonosov
Bluegene/P
Bluegene/P
Linear

Fig. 2

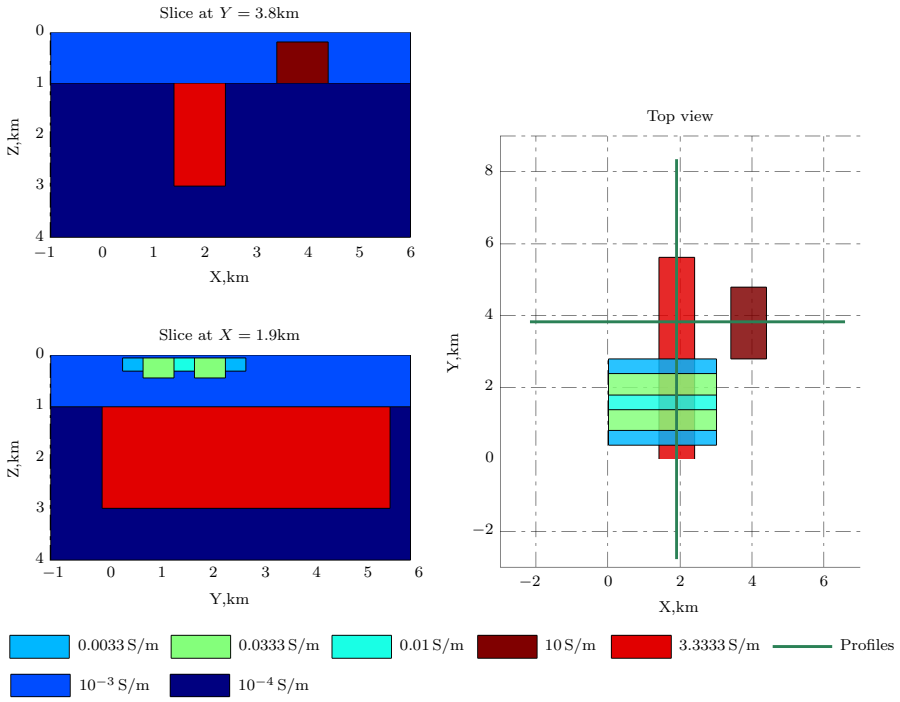
Slice at $Y = 3.8$km
Z,km
X,km
Slice at $X = 1.9$km
Z,km
Y,km
Top view
Y,km
X,km
0.0033 S/m
0.0333 S/m
0.01 S/m
10 S/m
3.3333 S/m
Profiles
10^{-3} S/m
10^{-4} S/m

Fig. 3

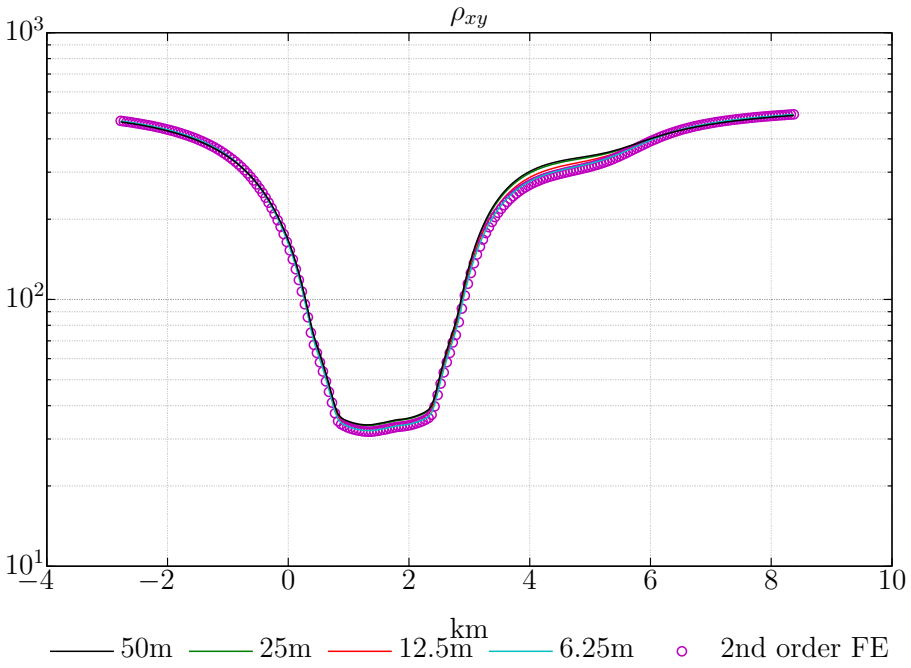

Fig. 4

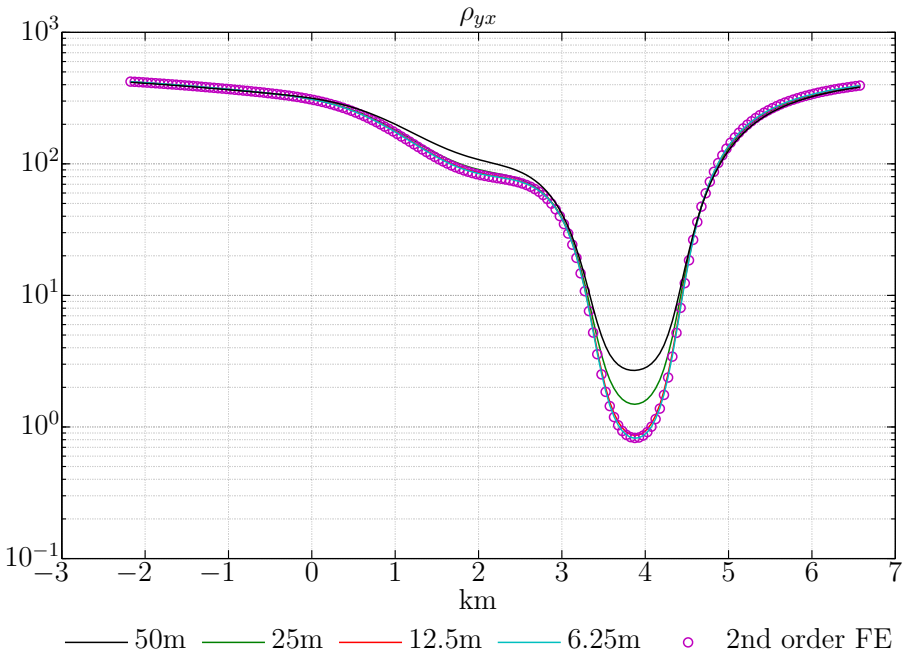
ρ_{yx}
10^3
10^2
10^1
10^0
10^{-1}
−3
−2
−1
0
1
2
3
4
5
6
7
km
50m
25m
12.5m
6.25m
2nd order FE

Fig. 5

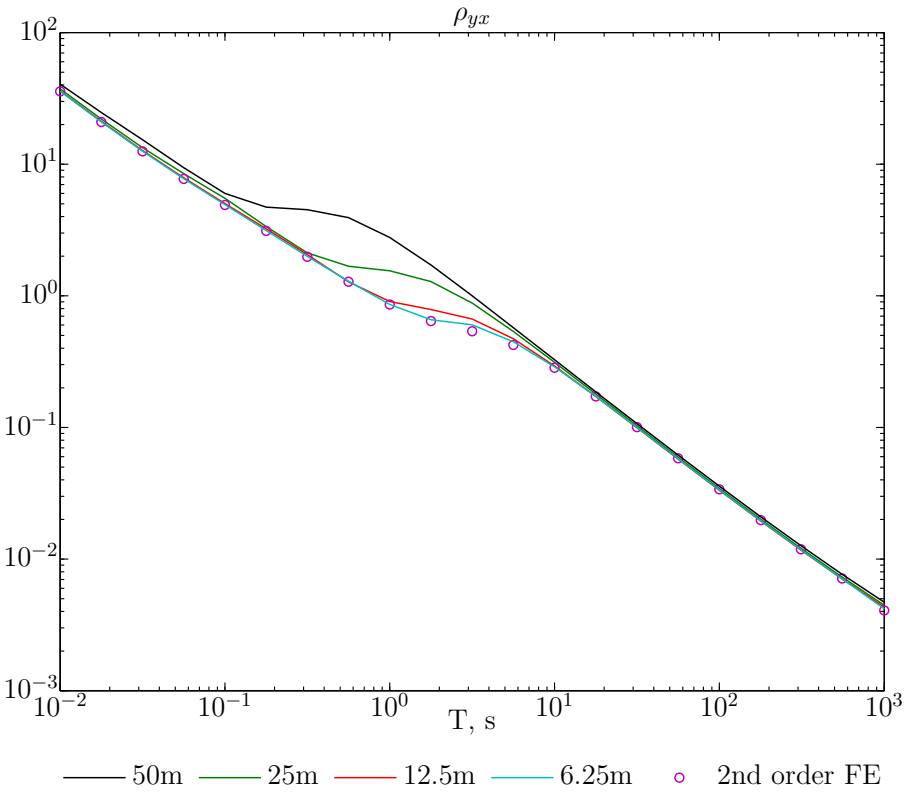
ρ_{yx}
10^2
10^1
10^0
10^{-1}
10^{-2}
10^{-3}
10^{-2}
10^{-1}
10^0
10^1
10^2
10^3
T, s
50m
25m
12.5m
6.25m
2nd order FE

Fig. 6

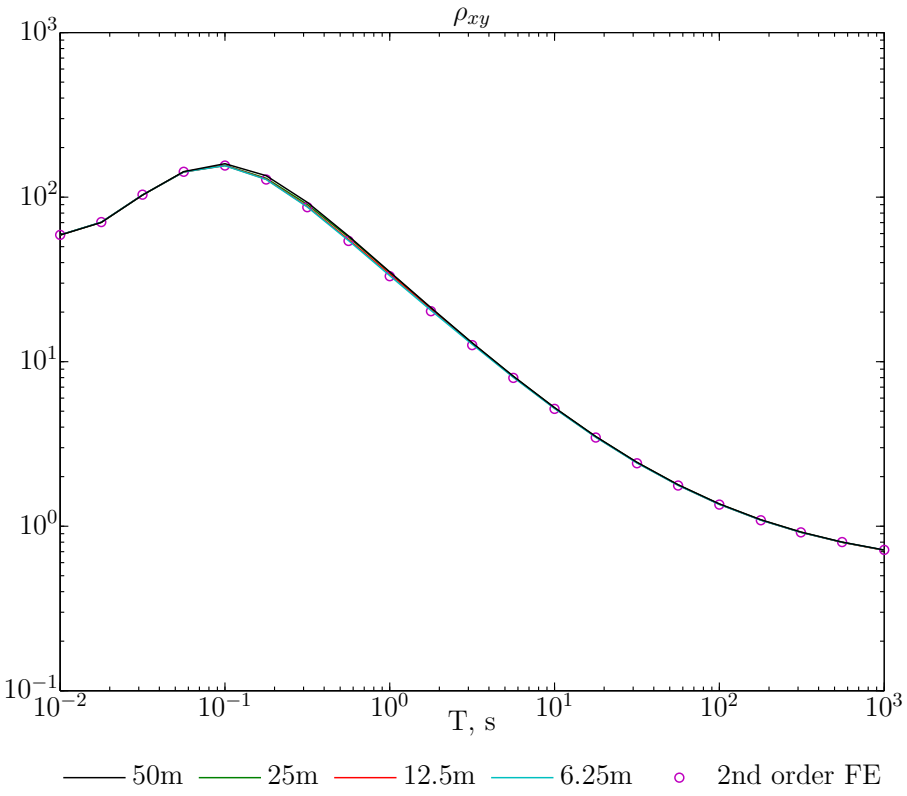
ρ_{xy}
10^3
10^2
10^1
10^0
10^{-1}
10^{-2}
10^{-1}
10^0
10^1
10^2
10^3
T, s
50m
25m
12.5m
6.25m
2nd order FE

Fig. 7

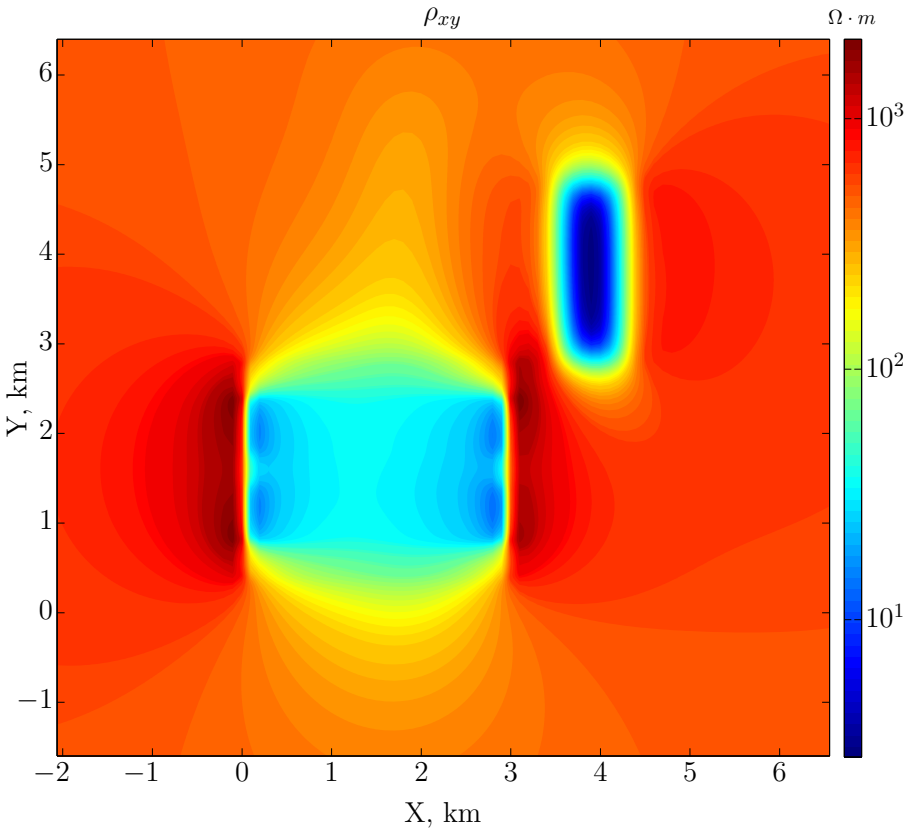

Fig. 8

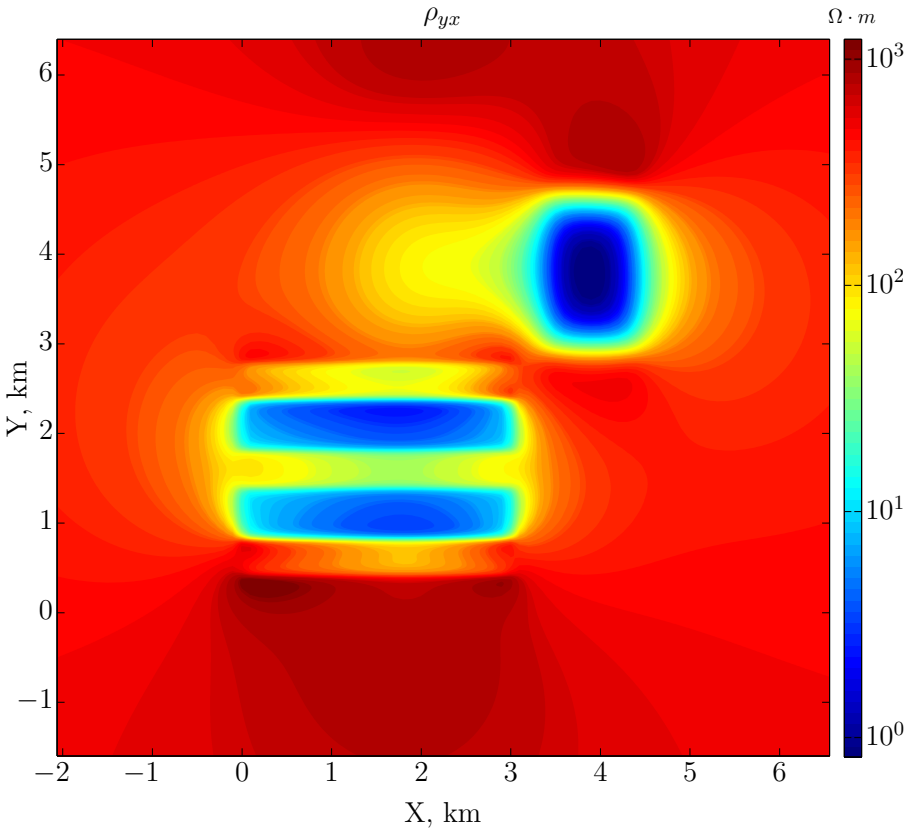
ρ_{yx}
$\Omega \cdot m$
10^3
10^2
10^1
10^0
Y, km
X, km
6
5
4
3
2
1
0
−1
−2
−1
0
1
2
3
4
5
6

Fig. 9

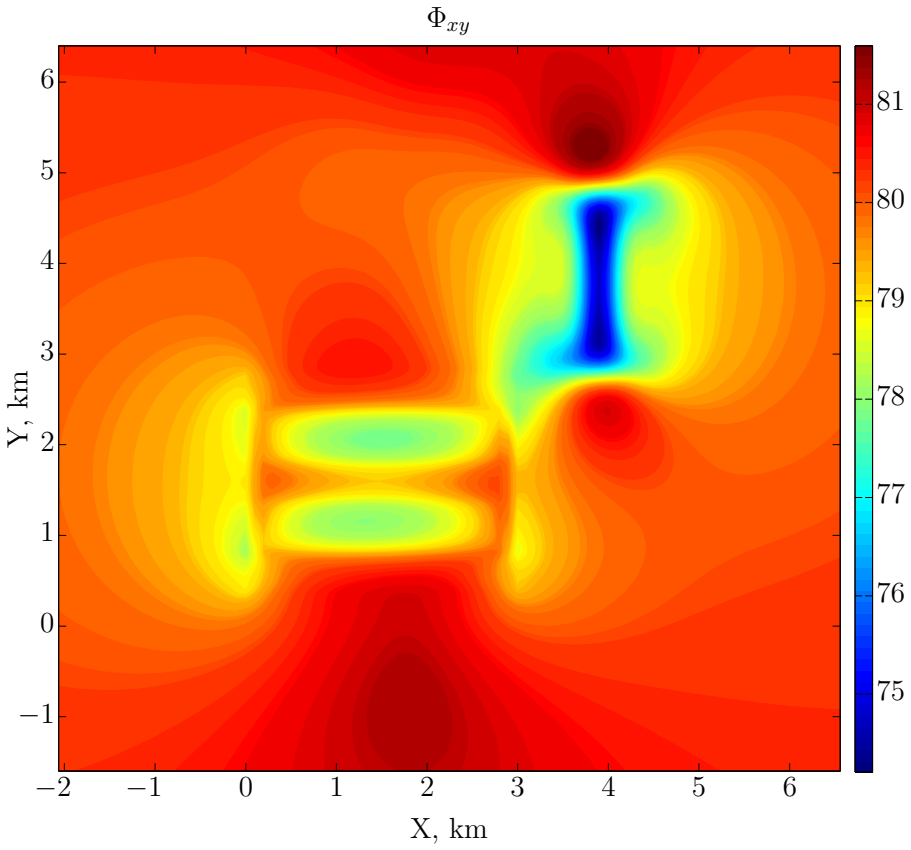

Fig. 10

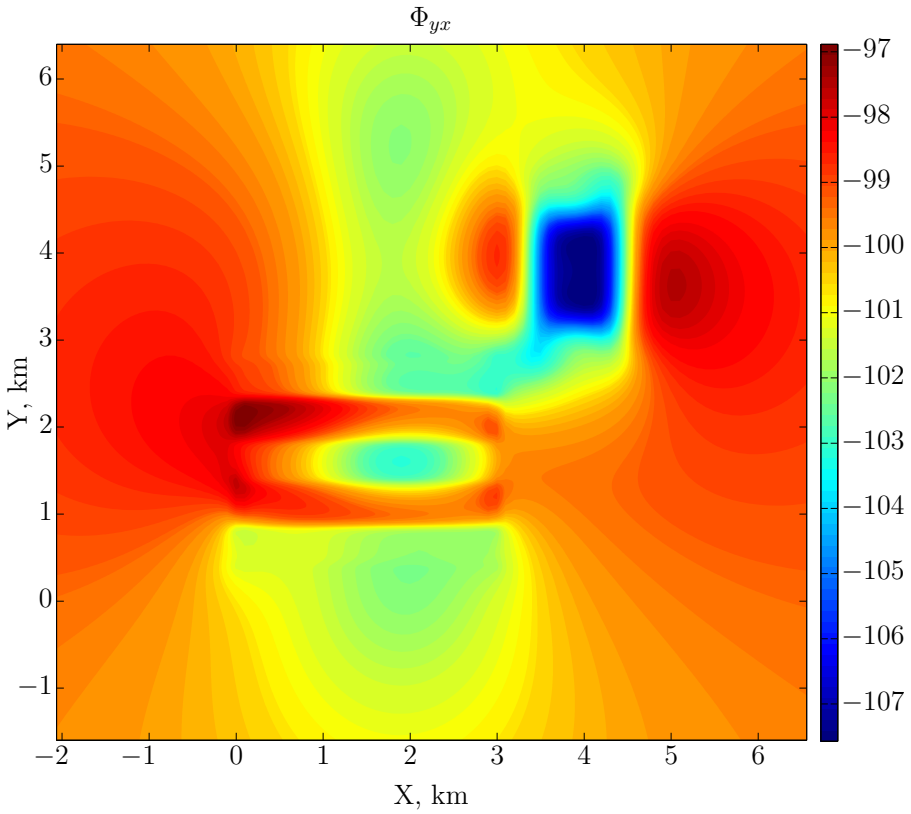
Φ_{yx}
Y, km
X, km
6
5
4
3
2
1
0
−1
−2
−1
0
1
2
3
4
5
6
−97
−98
−99
−100
−101
−102
−103
−104
−105
−106
−107

Fig. 11

List of Tables

Node 0	…	Node N_y-1	Node N_y	…	Node $2N_y-1$
$\widetilde{Q}(0,0)$	…	$\widetilde{Q}(N_y-1,0)$	$\widetilde{Q}(0,N_x/2)$	…	$\widetilde{Q}(N_y-1,N_x/2)$
$\widetilde{Q}(0,1)$	…	$\widetilde{Q}(N_y-1,1)$	$\widetilde{Q}(0,N_x/2+1)$	…	$\widetilde{Q}(N_y-1,N_x/2+1)$
$\vdots$	…	$\vdots$	$\vdots$	…	$\vdots$
$\widetilde{Q}(0,N_x/2-1)$	…	$\widetilde{Q}(N_y-1,N_x-1)$	$\widetilde{Q}(0,N_x-1)$	…	$\widetilde{Q}(N_y-1,N_x-1)$

Table 1

	x_1	y_1	z_1	x_2	y_2	z_2	σ
1	0	2.4	0.05	3	2.8	0.3	0.0033
2	0	1.8	0.05	3	2.4	0.45	0.033
3	0	1.4	0.05	3	1.8	0.30	0.1
4	0	0.8	0.05	3	1.4	0.45	0.033
5	0	0.4	0.05	3	0.8	0.30	0.0033
6	3.4	2.8	0.2	4.4	4.8	1	10
7	1.4	0	1	2.4	5.6	3	3.3333

Table 2